New Journal of Physics
The open–access journal for physics

Imaging of carrier-envelope phase effects in above-threshold ionization with intense few-cycle laser fields

M F Kling[1,2,6], J Rauschenberger[2,3], A J Verhoef[2], E Hasović[4], T Uphues[2], D B Milošević[4,5], H G Muller[1] and M J J Vrakking[1,6]

[1] FOM Instituut voor Atoom en Molecuul Fysica (AMOLF), Kruislaan 407, 1098 SJ Amsterdam, Netherlands.
[2] Max-Planck-Institut für Quantenoptik, Hans-Kopfermann-Strasse 1, 85748 Garching, Germany.
[3] Department für Physik, Ludwig-Maximilians-Universität München, Am Coulombwall 1, 85748 Garching, Germany.
[4] Faculty of Science, University of Sarajevo, Zmaja od Bosne 35, 71000 Sarajevo, Bosnia and Herzegovina.
[5] Max-Born-Institut, Max-Born-Strasse 2a, 12489 Berlin, Germany
E-mail: matthias.kling@mpq.mpg.de and m.vrakking@amolf.nl

New Journal of Physics **10** (2008) 025024 (17pp)
Received 2 October 2007
Published 29 February 2008
Online at http://www.njp.org/
doi:10.1088/1367-2630/10/2/025024

Abstract. Sub-femtosecond control of the electron emission in above-threshold ionization of the rare gases Ar, Xe and Kr in intense few-cycle laser fields is reported with full angular resolution. Experimental data that were obtained with the velocity-map imaging technique are compared to simulations using the strong-field approximation (SFA) and full time-dependent Schrödinger equation (TDSE) calculations. We find a pronounced asymmetry in both the energy and angular distributions of the electron emission that critically depends on the carrier-envelope phase (CEP) of the laser field. The potential use of imaging techniques as a tool for single-shot detection of the CEP is discussed.

[6] Authors to whom any correspondence should be addressed.

Contents

1. Introduction

Control of the electric field waveform of laser light pulses has opened a new way to study and control electron dynamics in strong-field processes. Laser light with controlled evolution of the electric field $E(t) = E_0(t) \cdot \cos(\omega t + \varphi_{\mathrm{CEP}})$ became available when, in addition to the amplitude $E_0(t)$ and frequency ω control of the carrier-envelope phase (CEP) φ_{CEP} was accomplished [1]. The well-controlled force varying on a sub-femtosecond timescale that such a wave exerts on electrons permitted the reliable and reproducible generation of single sub-femtosecond pulses [2] by means of high-order harmonic generation [3], and has been used to control electron emission from atoms [4–6] and the localization of electrons in a molecular dissociation reaction [7] and made precision attosecond metrology possible [8]. Many of these achievements have been a direct consequence of the capability of steering the motion of bound electrons in atoms as well as those having been set free from their atomic bound state. It follows that measurements of the carrier envelope phase of a few-cycle pulse, preferably performed *in situ*, have recently attracted considerable attention. One of the first absolute measurements of the CEP of a few-cycle laser pulse (employing the low-power output of a 24 MHz oscillator) was performed by Apolonski *et al* [9], and made use of the sensitivity of multi-photon surface photo-emission on a gold surface to the CEP of the irradiating few-cycle laser. Another realization of the measurement of the absolute phase was implemented by Paulus and coworkers using the observation of above-threshold ionization (ATI) in the strong-field ionization of several atomic species [6, 10, 11]. Recently, high-power and low-repetition rate CEP-measurements have been performed using terahertz generation [12], or using the observation of half-cycle cut-offs (HCOs) in high-order harmonic generation [13]. A driving force behind these studies has been the desire to perform a *single-shot* determination of the CEP of the laser system, while using only a moderate fraction of the available pulse energy. In the present paper, we explore to what extent a measurement of ATI using the velocity-map imaging (VMI) technique, where electrons are projected onto a two-dimensional (2D) position-sensitive detector, can be used towards this end.

ATI of rare gases has been studied intensively in the last decades (see, e.g., [14, 15] and references cited therein). Electrons in atoms that ionize by means of tunneling are accelerated in the oscillatory electric field of the ionizing laser and can reach a maximum kinetic energy

of $2U_p$, where the so-called ponderomotive energy $U_p = e^2 E_{laser}^2/(4\, m_e \omega^2)$ for a laser with the electric field amplitude E_{laser} [16]. DiMauro and co-workers [17, 18] and Paulus *et al* [19] found high-energy contributions in ATI spectra above $2U_p$ that were attributed to the rescattering of ionized electrons with energies of up to $10U_p$ [19]. Paulus *et al* have also performed ATI with waveform-controlled few-cycle laser pulses (for a recent review see [15]). For few-cycle pulses the electron emission was found to be asymmetric along the laser polarization direction and to strongly depend on the value of the CEP [6, 10, 20]. For the highest electron energies approaching the $10U_p$ cut-off, the CEP serves as a control parameter to steer the electron emission up or down along the laser polarization [5, 6]. At lower energies, where more than a single trajectory can contribute, Lindner *et al* [4] observed a clear dependence of the ATI interference patterns on the CEP.

The type and amount of information that can be extracted from the electrons that leave an atom, molecule, cluster or nanoparticle upon irradiation, is crucial for the understanding of the processes that led to their release. These properties, in turn, have a profound effect on the final properties (kinetic energy and angular distribution) of the electrons that can be measured. For instance, it was shown that a suitable interference of attosecond electron wave packets generated in the continuum by ionization may yield information on the wavefunction of the system [21]. In addition, it has been proposed that recording the angle- and energy-resolved photoelectron spectrum for strong-field ionization of a molecule may reveal the structure of the molecule [22]. VMI is a technique that efficiently allows the collection of such information. In VMI, originally developed by Chandler and Houston in 1987 [23] and significantly improved by Eppink and Parker in 1997 [24], the full 3D-momentum distribution of electrons (or ions) can be reconstructed from a 2D-projection recorded by a MCP/phosphor screen/CCD-camera detection system [25].

Angular resolved studies of the electron emission in ATI have been less abundant than measurements at selected angles. Helm and co-workers introduced the VMI technique into atomic photoionization experiments [26]. Correlating the number of minima in the observed angular distributions with the angular momentum of a resonant intermediate state, their work clearly showed the effect of Freeman resonances on the ionization dynamics. Angular distribution measurements of electrons in the lower energy region have also been the subject of detailed investigations by Nandor *et al* [27] while angular distribution measurements in the high energy plateau region were performed by Yang *et al* [18] and Paulus *et al* [28]. They observed that electrons were ejected between 30° and 45° with respect to the laser polarization axis. These side-lobes in the angular distributions were attributed to rescattering processes [19, 29]. No study so far has appeared on angle-resolved ATI measurements with waveform-controlled few-cycle pulses.

In this paper, we will present experimental data that have been recorded for ATI of the rare gases argon, krypton and xenon in strong few-cycle laser fields using the VMI technique. We will discuss the dependence of asymmetries in the angular and energy distributions of the electron emission on the CEP of the laser. The data for argon are compared to time-dependent Schrödinger equation (TDSE) and strong-field appoximation (SFA) simulations. In the last part of the paper, the possibility of performing single-shot CEP measurements by means of VMI of ATI is discussed.

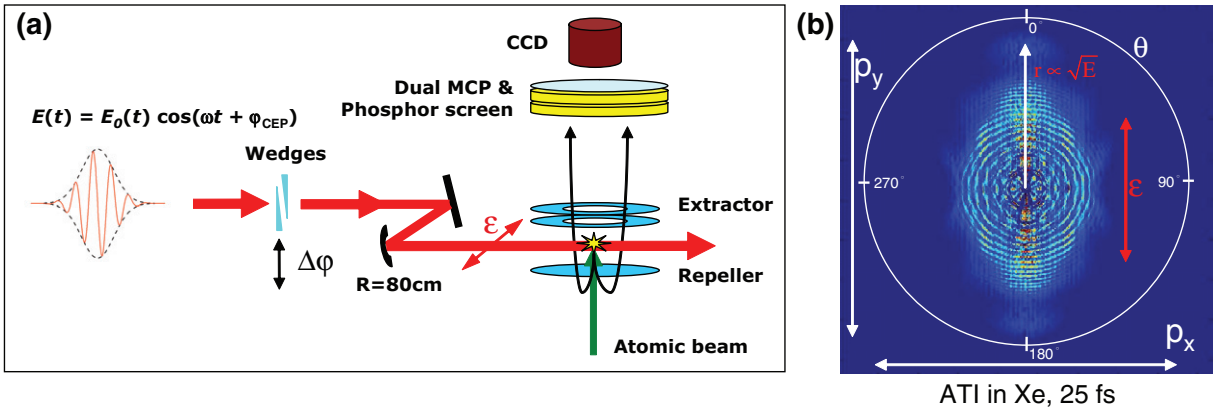

Figure 1. (a). Schematic of the experimental set-up. (b) Inverted image of ATI in xenon for 25 fs laser pulses at 10^{14} W cm^{-2}.

2. Experiment

The experimental scheme that was used for the detection of absolute phase effects in the ATI of rare-gases is displayed in figure 1(a). Transform-limited laser pulses of 25 fs duration with 1 mJ pulse energy were generated with a 3 kHz phase-stabilized amplified Ti:sapphire laser system (Femtolasers, Femtopower Compact Pro). The pulse bandwidth was subsequently broadened in a one-meter long neon-filled hollow-core fiber. The output pulses from the fiber were compressed to near-transform-limited duration in a chirped mirror compressor. The pulse duration could be varied between 5 and 25 fs by tuning the gas pressure in the hollow-core fiber. The laser phase was stabilized with a feedback loop as detailed in [30]. Phase-stabilized and linearly polarized pulses at a central wavelength of 760 nm were focused into the center of the electron optics of a VMI apparatus using a spherical mirror ($R = 80$ cm). In the focus intensities up to 5×10^{14} W cm^{-2} were realized, and an adjustable iris was used to vary the intensity.

Electrons that were generated at the crossing point of the laser (the x-axis) and an atomic beam (the z-axis) were accelerated and focused with the electron optics onto an MCP-phosphor screen assembly (Hamamatsu, F2226-24PX). The polarization of the laser was chosen along the y-axis, i.e. parallel to the xy-plane of the MCP detector. The atomic beam was operated at 50 Hz and the MCP was switched such that electrons from every 60th laser pulse were detected. This allowed maintaining a low background pressure in the chamber (typically 2×10^{-7} mbar) and kept ionization from background gases and rare gas atoms that were not part of the atomic beam sufficiently low. Images were recorded with a CCD camera (Pulnix, TM-9701) and typically averaged over 1 min of data acquisition for each phase. Note that in order to be able to measure the plateau electrons clearly, the detector has been driven into saturation in the center (contributions below 1 eV). 3D-momentum distributions $P(p, \theta, \phi)$ (where p is the momentum and the polar and azimuthal angles θ and ϕ are defined with respect to the laser polarization axis) were obtained by means of an iterative inversion procedure [25]. Figure 1(b) shows a cut through the 3D-momentum distribution in Cartesian coordinates (p_x, p_y) at $p_z = 0$ that was recorded for ATI in xenon with 25 fs pulses at 10^{14} W cm^{-2} without phase stabilization. The laser polarization along the y-axis ($\theta = 0^\circ/180^\circ$) is indicated in the figure. The picture shows that in momentum space all photo-ionized electrons lie on concentric rings, consistent with the fact that ATI occurs where electrons are formed with a kinetic energy $W = n\hbar\omega - IP - U_p$,

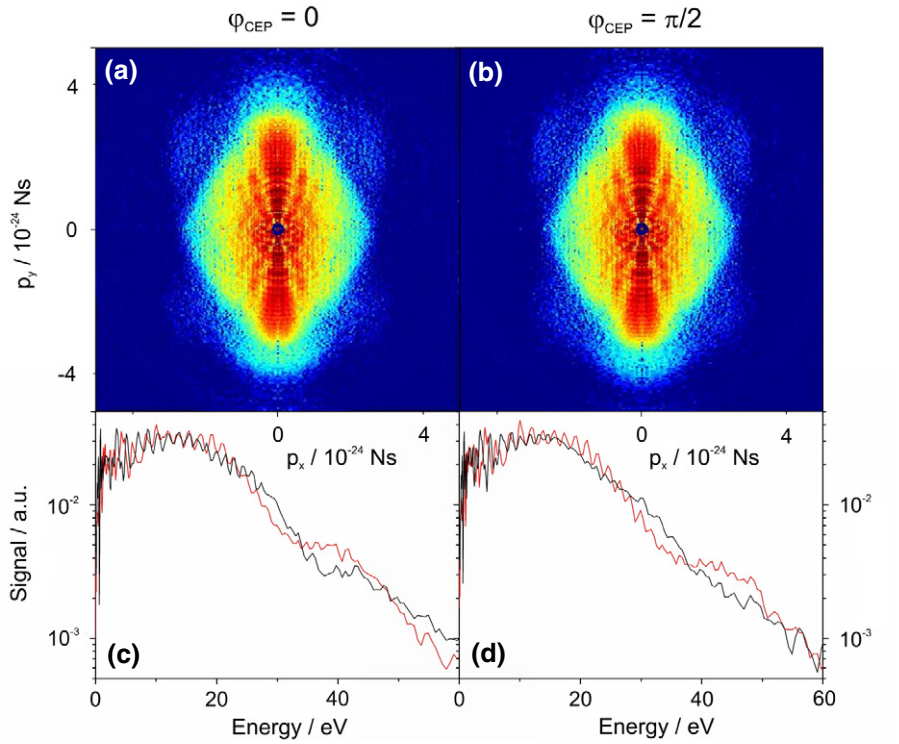

Figure 2. (a), (b) Inverted images for ATI of argon with 6 fs laser pulses at $10^{14}\,\mathrm{W\,cm^{-2}}$ for phases of $\varphi_{\mathrm{CEP}} = 0$ and $\varphi_{\mathrm{CEP}} = \pi/2$, measured by VMI. Photoelectrons are accelerated towards a 2D detector where their positions of impact are recorded, and where faster electrons are detected further from the center; in this case, the sharper structures correspond to interferences of electron trajectories. (c), (d) Electron kinetic energy spectra obtained from angular integration over an angular range of 40° along the laser polarization direction (vertical) in the two images above; black curves: emission upwards, red curves: emission downwards.

where *IP* is the ionization potential of the atom under investigation and *n* is the number of absorbed photons. The image shows that the ATI electrons are preferentially emitted along the laser polarization axis, although the side-lobes between 30° and 45° that were previously reported [18, 28] and highly oscillatory angular distributions at low energy that indicate the role of Freeman resonances [26] are clearly visible as well.

3. CEP effects in few-cycle ATI of argon

Figure 2 displays two cuts through the 3D-momentum distribution along the $p_z = 0$ plane of the emission for electrons resulting from ATI of argon with 6 fs pulses at an intensity of $10^{14}\,\mathrm{W\,cm^{-2}}$ ($U_\mathrm{p} = 5.4\,\mathrm{eV}$) for the phases $\varphi_{\mathrm{CEP}} = 0$ and $\pi/2$. Note that here and in all measurements described below only a relative phase shift between individual images was measured and $\varphi_{\mathrm{CEP}} = 0$ has been set according to a maximum in the asymmetry for the cut-off electrons (as detailed below). $\varphi_{\mathrm{CEP}} = 0$ corresponds to a cosine-like waveform, whereas

$\varphi_{\mathrm{CEP}} = \pi/2$ corresponds to a sine-like waveform. Panels (c) and (d) of figure 2 show the corresponding photoelectron spectra for the emission in the upward (black) and downward (red) directions, respectively. The spectra result from integration within a 40° angular range along the polarization direction. In agreement with expectations based on earlier observations [6], the highest energy contributions for a cosine-like waveform (figure 2(c)) are different for the two emission directions and similar for a sine-like waveform (figure 2(d)). This behavior stems from the fact that the maximum electric field amplitudes in the two emission directions for $\varphi_{\mathrm{CEP}} = 0$ are significantly different while they are the same for $\varphi_{\mathrm{CEP}} = \pi/2$. In agreement with earlier observations, the CEP dependent changes in the spectra are most pronounced in the high energy region of the spectrum (beyond $2U_{\mathrm{p}}$). Interference fringes at energies below the cutoff (in the data here clearly visible up to approximately $5U_{\mathrm{p}}$) are indicative of the contribution of more than a single electron trajectory to a final position in momentum space. Side-lobes in the angular distributions in figures 2(a) and (b) are observed between 30° and 60°. Such side-lobes have been attributed earlier to rescattering effects [19, 29].

In order to reveal the phase dependence in the upward/downward electron emission, images were recorded while changing the CEP over a range of 4π with a step size of $\Delta\varphi_{\mathrm{CEP}} = 0.2\pi$. The angle-integrated asymmetry in the electron emission was evaluated as a function of energy $W = p^2/(2m_{\mathrm{e}})$ and laser phase φ_{CEP} via

$$A(W, \varphi_{\mathrm{CEP}}) = \frac{P_{\mathrm{up}}(W, \varphi_{\mathrm{CEP}}) - P_{\mathrm{down}}(W, \varphi_{\mathrm{CEP}})}{P_{\mathrm{up}}(W, \varphi_{\mathrm{CEP}}) + P_{\mathrm{down}}(W, \varphi_{\mathrm{CEP}})} \tag{1}$$

with

$$\mathrm{P}_{\mathrm{up}}(W, \varphi_{\mathrm{CEP}}) = \int_{340^\circ}^{360^\circ} \mathrm{P}(W, \theta, \varphi_{\mathrm{CEP}})\,\mathrm{d}\theta + \int_{0^\circ}^{20^\circ} \mathrm{P}(W, \theta, \varphi_{\mathrm{CEP}})\,\mathrm{d}\theta$$

and

$$\mathrm{P}_{\mathrm{down}}(W, \varphi_{\mathrm{CEP}}) = \int_{160^\circ}^{200^\circ} \mathrm{P}(W, \theta, \varphi_{\mathrm{CEP}})\,\mathrm{d}\theta.$$

Figure 3(a) shows the asymmetry map $A(W, \varphi_{\mathrm{CEP}})$ for ATI in argon as recorded for the parameters given above. A clear oscillation of the asymmetry with CEP is seen in the energy range between 20 and 60 eV, corresponding to the plateau part of the spectrum. At a given kinetic energy the asymmetry oscillation can be fitted as a cosine function according to $A(W, \varphi_{\mathrm{CEP}}) = A_0(W)\cos(\varphi_{\mathrm{CEP}} - \varphi_{\mathrm{asymmetry}}(W))$. A clear shift of the phase of the asymmetry oscillation $\varphi_{\mathrm{asymmetry}}(W)$ with energy is evident from the slope in the red (emission up) and blue (emission down) features in figure 3(a). Similar patterns were observed and predicted in classical calculations by Paulus *et al* [6]. A measurement of the oscillation of the asymmetry at two different energies or a measurement of the asymmetry at the highest electron energy in addition to a measurement of the total electron yield can thus be utilized to determine the absolute phase of a laser pulse without $\pm\pi$ ambiguity [6, 11].

The asymmetry was also evaluated without angular integration, i.e. as $A(W, \theta, \varphi_{\mathrm{CEP}})$ and for each value of the energy W and angle θ fit to the function $A(W, \theta, \varphi_{\mathrm{CEP}}) = A_0(W, \theta)\cos(\varphi_{\mathrm{CEP}} - \varphi_{\mathrm{asymmetry}}(W, \theta))$. Figure 3(b) shows the shift of the phase $\varphi_{\mathrm{asymmetry}}(W, \theta)$

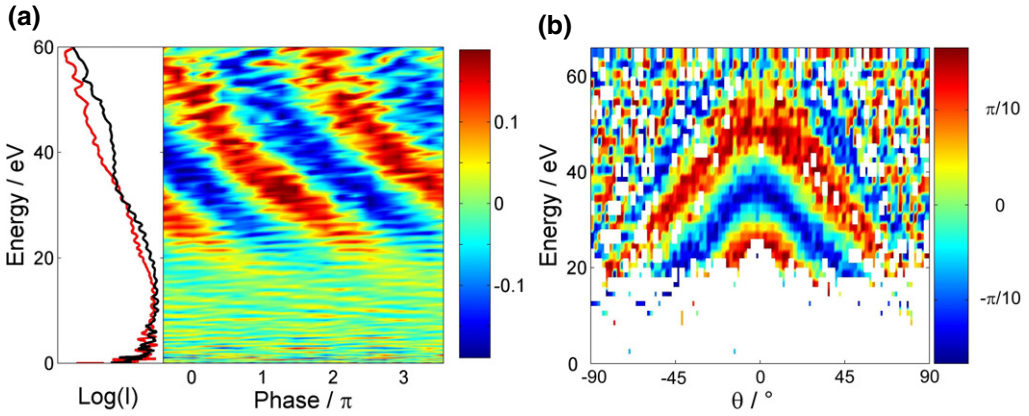

Figure 3. (a) Left side: spectra for ATI in argon for $\varphi = 0$ in the up (black) and down (red) directions. Right side: Asymmetry map $A(W, \varphi_{\mathrm{CEP}})$ of the electron emission (red = preferentially upwards, blue = preferentially downwards) obtained from experimental data in argon (as shown in figure 2) by recording a series of images where φ_{CEP} is varied. The map shows that the emission direction can be controlled with the CEP. (b) Phase shift $\varphi_{\mathrm{asymmetry}}$ in the asymmetry $A(W, \theta, \varphi_{\mathrm{CEP}})$ oscillation with φ_{CEP} (only displayed for asymmetry amplitudes larger than 0.07, θ is given with respect to the polarization axis). The phase in the asymmetry oscillation depends strongly on both energy and angle of the emission.

in the asymmetry oscillation as a function of the energy W and angle θ. The phase shift $\varphi_{\mathrm{asymmetry}}(W, \theta)$ is only plotted for significantly high amplitudes of the asymmetry ($A_0(W, \theta) > 0.07$). In the region of the direct emission of electrons (up to $2U_{\mathrm{p}}$), in good agreement with the representation in figure 3(a), the amplitude of the asymmetry oscillation is very weak. The weak asymmetry of the low-energy electrons can be explained by their deflection in the oscillating laser field that cancels the initial nonlinear dependence of the ionization yield on the field strength [30]. In the plateau region of the presented argon data in figure 3, the asymmetry is larger and the phase of its oscillation with CEP $\varphi_{\mathrm{asymmetry}}(W, \theta)$ shifts not only with the electron kinetic energy W but also with the emission angle θ. The triangular patterns suggest that the observation of the asymmetry at a constant energy but two different emission angles can also serve as a way to measure the phase φ_{CEP} of the laser pulse without $\pm\pi$ ambiguity.

4. TDSE and SFA simulations on CEP effects in few-cycle ATI of argon

In order to better understand the observations made in the present experiments, angle-resolved ATI spectra were calculated, based on a generalization of the SFA theory introduced by Keldysh [31]. In this approach, the influence of the binding potential is neglected once the electron is emitted and the ionized electron wavefunction is described by a Volkov state. The improved SFA treatment includes one act of rescattering of the ionized electron wave packet off the parent ion (for more details see the review articles [14, 32]), which is responsible for the high-energy electron spectrum (its plateau and cutoff). A further generalization of the SFA theory and the method of focal averaging for infinitely long pulses was presented in [33].

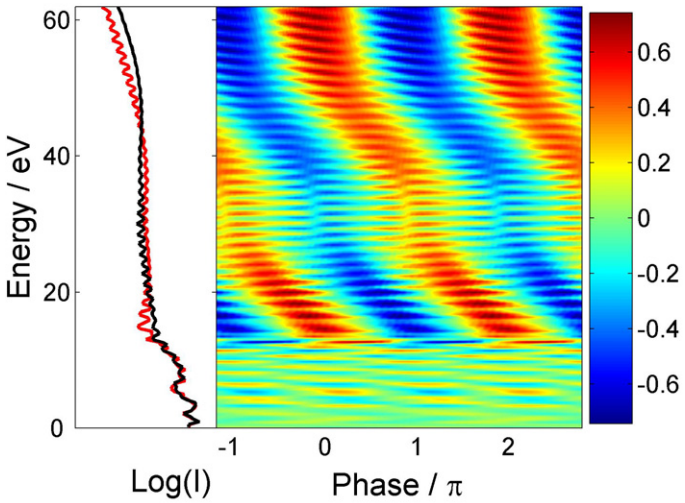

Figure 4. Left side: SFA calculated spectra for ATI in argon for 6.5 fs pulses at an intensity of $10^{14}\,\mathrm{W\,cm^{-2}}$ and $\varphi_{\mathrm{CEP}} = 0$ in the up (black) and down (red) directions. Note that the displayed data are obtained after volume integration. Right side: asymmetry map $A(W, \varphi_{\mathrm{CEP}})$ resulting from calculations for various values of φ_{CEP}.

In the present paper for ATI by few-cycle pulses a further generalization of the theory, presented in [14, 32, 33], was applied. In the review article [15] the improved SFA theory of ATI by few-cycle pulses was introduced, which is now combined with a realistic modeling of the ground-state wavefunction and a realistic rescattering potential for inert gases as presented in [33]. The focal-averaging method of [33] is also modified. For a fixed laser intensity I the differential ionization probability for the emission of an electron with the momentum $\mathbf{p}$ is denoted by $w(\mathbf{p}, I)$. The focal-averaged electron signal $S(\mathbf{p}, I_{\mathrm{max}})$ is then obtained by integration of $w(\mathbf{p}, I)$ over the laser-focus volume element from zero intensity to the peak intensity I_{max}.

The main problem of the improved SFA calculations is that they neglect the long-range Coulomb interaction of the ionized electron with the ion. This is the main reason why they fail in describing the low-energy spectra of neutral atoms[7]. High-energy spectra are, however, reproduced quite well. A comparison with numerical *ab initio* TDSE calculations was presented in [15, 35]. The upper half of the SFA energy spectra agrees very well with the TDSE spectra for all phases [35].

The calculations were performed for argon ($m = 0$) at a laser peak intensity of $10^{14}\,\mathrm{W\,cm^{-2}}$ at 760 nm with a pulse duration of 6.5 fs. Figure 4 displays two spectra at $\varphi_{\mathrm{CEP}} = 0$ in the up and down directions of the electron emission and the asymmetry map $A(W, \varphi_{\mathrm{CEP}})$ over a phase range of 4π. Slopes in the asymmetry oscillations with energy are seen that agree reasonably well with the experimental data above 40 eV, however, the phase jump around 30–35 eV was not observed in the experiments. Such a phase jump was also observed earlier in SFA calculations [35] and it is noteworthy that it has survived focal averaging. The phase jump has its origin in an

[7] For short-range interaction which characterizes the negative ions the improved SFA works extremely well; see [34].

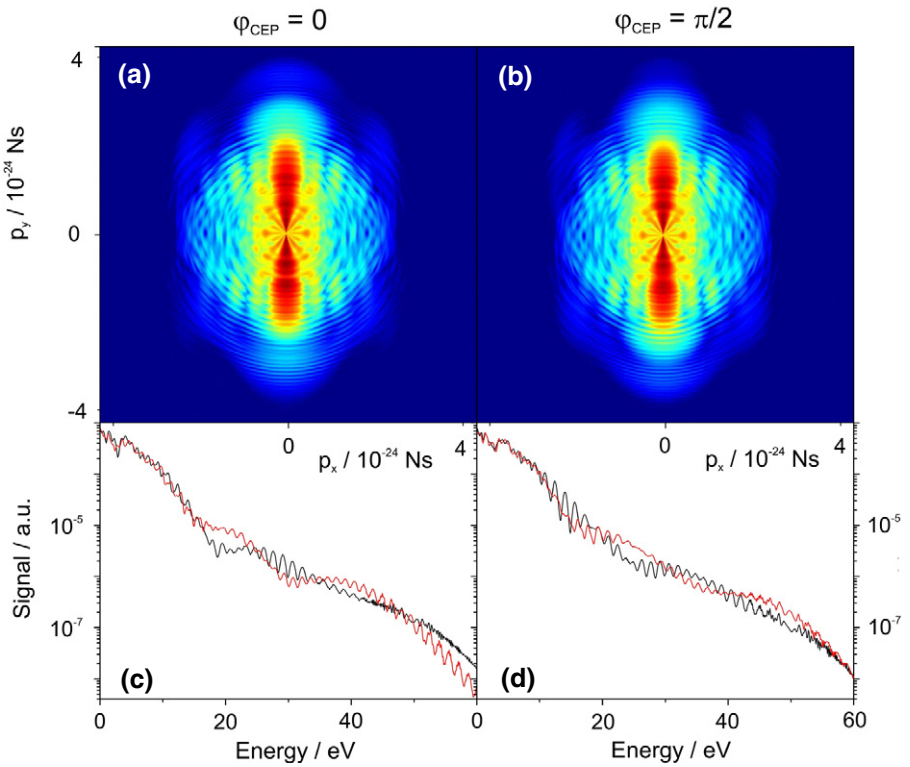

Figure 5. (a), (b) 2D-momentum representation of TDSE calculations for argon for phases $\varphi_{\mathrm{CEP}} = 0$ and $\varphi_{\mathrm{CEP}} = \pi/2$. The displayed data have been obtained after volume integration of single intensity calculations for 5.8 fs pulses at a peak intensity of $10^{14}\,\mathrm{W\,cm^{-2}}$. (c), (d) Electron kinetic energy spectra obtained from angular integration over an angular range of 40° along the laser polarization direction (vertical) in the two images above; black curves: emission upwards, red curves: emission downwards.

interference of a few saddle-point solutions, whose contributions to the ionization probability change with the electron energy and the CEP [15].

Calculations were also performed for argon solving the TDSE in the single-active electron approximation. Argon 3p ($m = 0, 1$) atoms were exposed to a few-cycle $\omega_{\mathrm{laser}} = 0.057$ au (800 nm) sin-squared laser pulse with a chosen CEP, a peak value of the vector potential ranging from 0.4 to 1.25 au, and a variable number of cycles ranging from 2 to 8. Best agreement was obtained when using 6 cycles (corresponding to a pulse duration of 5.8 fs), and only these results will be considered henceforth. The electronic wavefunction was propagated in the velocity gauge, using a grid employing 6×10^4 radial gridpoints and angular momenta up to $L = 25$. The radial gridstep was fixed to 0.2 au. The angle-resolved photoelectron spectrum was computed up to an energy of 4 au and used to determine volume-integrated spectra that could be compared to the experiment. In figure 5, two momentum maps are shown that were calculated for $\varphi_{\mathrm{CEP}} = 0$ (figure 5(a)) and $\varphi_{\mathrm{CEP}} = \pi/2$ (figure 5(b)) for conditions approximating the experiment, i.e. 6 fs laser pulses focused to a peak intensity of $10^{14}\,\mathrm{W\,cm^{-2}}$. Photoelectron kinetic energy distributions in the upward and downward directions along the laser polarization axis were obtained by integrating the volume-integrated angle-resolved photoelectron spectrum

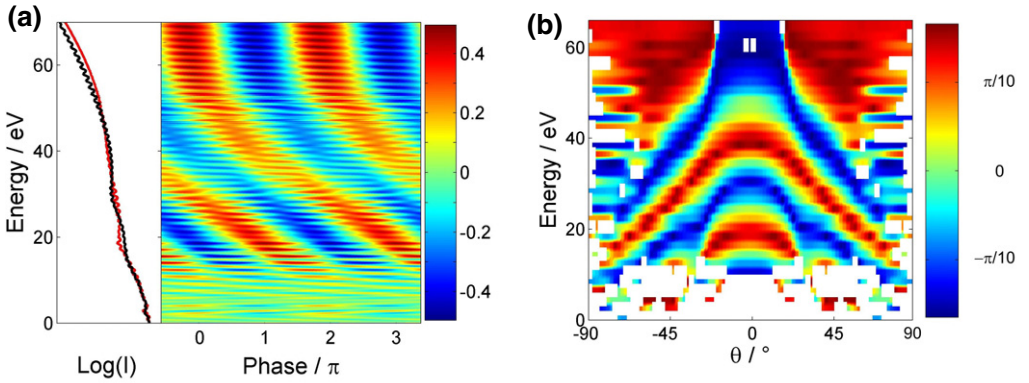

Figure 6. (a) Asymmetry map $A(W, \varphi_{\mathrm{CEP}})$ obtained from TDSE calculations for 5.8 fs pulses at an intensity of $10^{14}\,\mathrm{W\,cm^{-2}}$. Spectra are shown for $\varphi = 0$ and the emission in the up (black) and down (red) directions on the left side. (b) Phase shift $\varphi_{\mathrm{asymmetry}}$ in the asymmetry $A(W, \theta, \varphi_{\mathrm{CEP}})$ oscillation with φ_{CEP} (only displayed for asymmetry amplitudes larger than 0.07, θ is given with respect to the polarization axis). The triangular pattern in the phase shift that is determined from TDSE calculations resembles the experimental data given in figure 3(b).

within 40° along the laser polarization axis, and are shown in figures 5(c) and (d). Figure 5 reveals how the angle-resolved photoelectron spectra depend on the CEP and suggests that these distributions can be used for CEP retrieval purposes. While the cutoff of the re-collision plateau differs markedly in the upward and downward directions for $\varphi_{\mathrm{CEP}} = 0$, the cutoff is very similar in the case of $\varphi_{\mathrm{CEP}} = \pi/2$. Consistent with earlier observations, the CEP-dependent changes are most marked in the high-energy region of the spectrum (beyond $2U_{\mathrm{p}}$).

Results from performing CEP-dependent TDSE calculations at a large number of values of the CEP are collected in figure 6. In figure 6(a), an angle-integrated asymmetry parameter is plotted (calculated from the numerical results using equation (1)). In agreement with the experimental results of figure 3(a), figure 6(a) shows that at photoelectron energies beyond $2U_{\mathrm{p}}$ the angle-asymmetry parameter oscillates as a function of the CEP, with a relative phase that is determined by the photoelectron kinetic energy. Hence, a measurement of the angle-integrated asymmetry at two energies suffices to determine the CEP. Figure 6(b) displays the phase shift $\varphi_{\mathrm{asymmetry}}(W, \theta)$ of the asymmetry oscillation $A(W, \varphi_{\mathrm{CEP}})$. The triangular pattern in the phase shift that was observed in the experiments (see figure 3(b)) is retrieved very well by the TDSE calculations.

A more detailed comparison of the asymmetries in the electron emission in ATI in argon that have been determined from the measurements and the SFA and TDSE calculations is given in figure 7. The amplitude $A_0(W)$ and phase $\varphi_{\mathrm{asymmetry}}(W)$ of the energy-dependent asymmetry oscillations $A(W, \varphi_{\mathrm{CEP}}) = A_0(W)\cos(\varphi_{\mathrm{CEP}} - \varphi_{\mathrm{asymmetry}}(W))$ are shown for the three cases in figures 7(a) and (b), respectively. While the energy-dependent amplitudes of the asymmetry are similar for the SFA and TDSE calculations, they both do not agree well with the experimental data. In the experiments, the highest degree of asymmetry is observed between 20 and 60 eV (with a maximum at around 35 eV), while in both calculations the first maximum in the asymmetry is seen at approximately 20 eV and keeps increasing beyond 35 eV (note that the

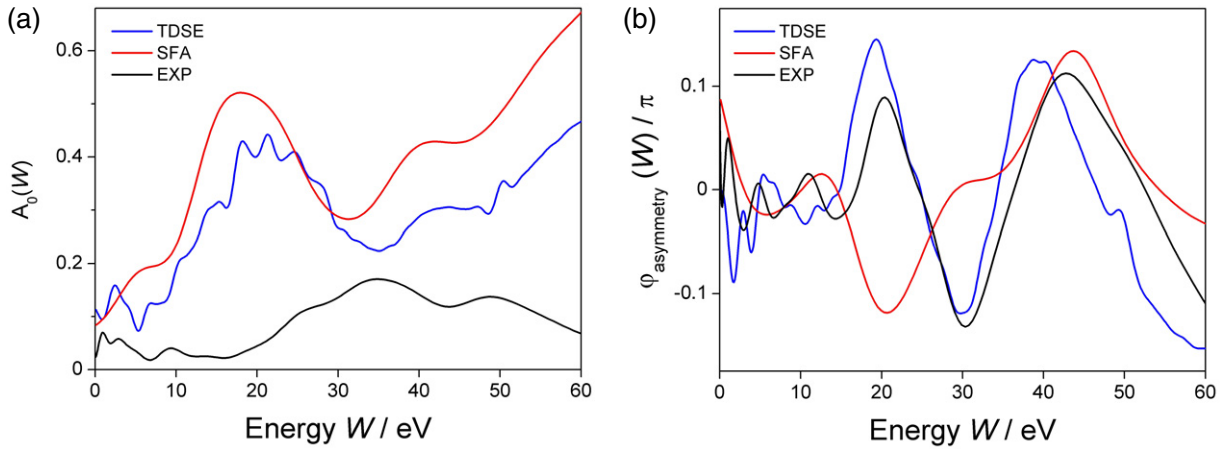

Figure 7. Asymmetry parameters $A_0(W)$ (left panel (a)) and $\varphi_{\text{asymmetry}}(W)$ (right panel (b)) according to a fit of the experimental (EXP), TDSE and SFA data to the function $A(W, \varphi_{\text{CEP}}) = A_0(W)\ \cos(\varphi_{\text{CEP}} - \varphi_{\text{asymmetry}}(W))$. Note that for clarity fast oscillations present in the data were suppressed in (a) and (b) by Fourier-filtering and that the determination of the absolute phase in the experimental data is based on an analysis of the cut-off electron asymmetries while this number is precisely known in the calculations.

spectral intensity in this region is, however, decreasing). Laser intensity variations and detector saturation or efficiency are not included in the calculations and may have decreased the visibility of the asymmetry at lower energies in the experiments. At high energies close to the cutoff region the number of counts in the experimental data reaches the limit of background noise (which exhibits no CEP dependence), such that the contrast in the asymmetry oscillation is reduced. This might explain the difference between the experimental data and the calculations in the cutoff region.

The pronounced shift in the phase $\varphi_{\text{asymmetry}}(W)$ that is seen in the experimental data (black line in figure 7(b)) is reproduced well beyond 35 eV by both the SFA and TDSE calculations. While a phase jump is visible for the SFA calculated asymmetries at around 30–35 eV, the difference between the TDSE calculated values and the experimental data stays consistently below 0.1 rad and thus shows excellent agreement all the way down to about $2U_{\text{p}}$ (below this value, noise dominates the curves due to the low amplitude of the asymmetry).

5. CEP effects in few-cycle ATI of krypton and xenon

We have also studied the CEP dependence of the electron emission in ATI of krypton and xenon in intense few-cycle laser fields. Figures 8(a) and (b) show inverted images for krypton that have been obtained from the experimental 2D-projections for $\varphi_{\text{CEP}} = 0$ and $\pi/2$ for 6 fs pulses at an intensity of 10^{14} W cm^{-2}. A contour plot showing the asymmetry of the photoelectron spectrum integrated within a cone of 40° along the polarization axis as a function of the photoelectron kinetic energy and the CEP is shown in figure 8(c). Two spectra taken at $\varphi_{\text{CEP}} = 0$, in the upward (black) and downward (red) directions (integrated over angular ranges of 40° along the vertical laser polarization axis), are shown in the left panel in figure 8(c), which show good agreement with previously recorded few-cycle ATI spectra for krypton within this intensity range [36].

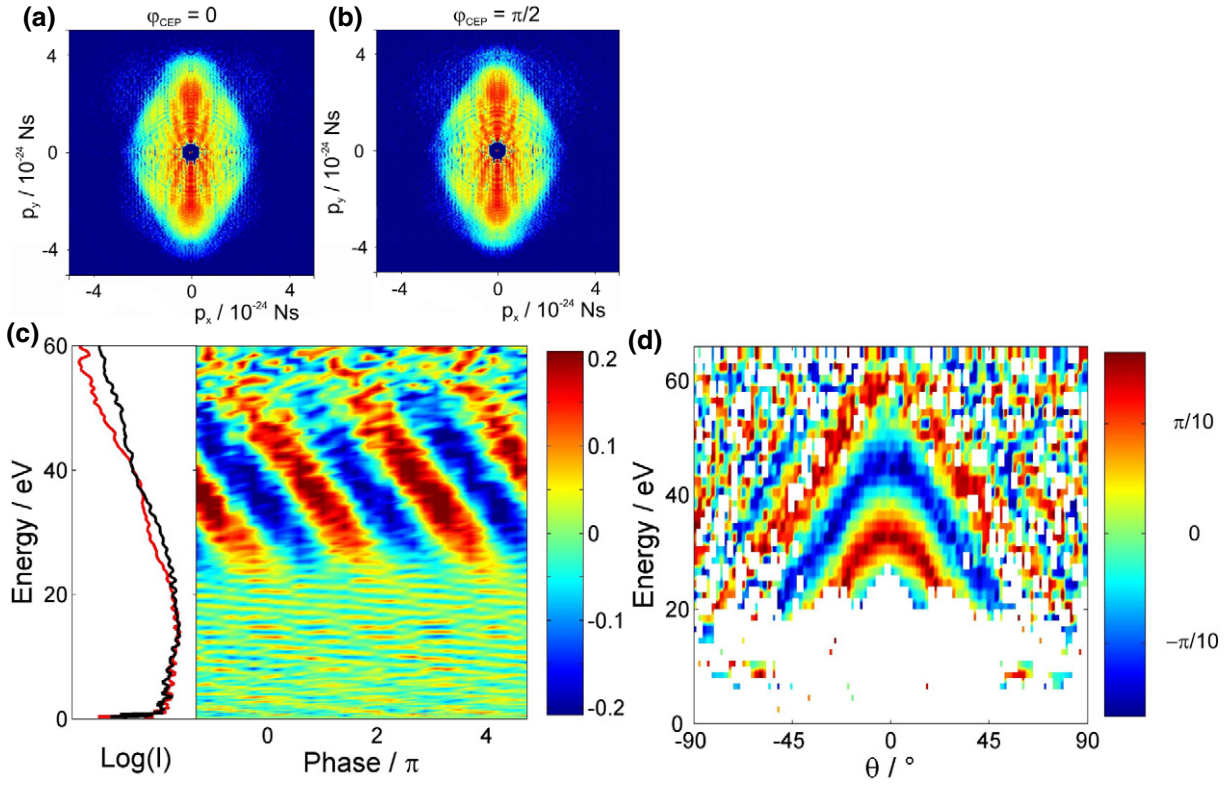

Figure 8. (a), (b) Inverted images for ATI of krypton with 6 fs laser pulses at $10^{14}\,\mathrm{W\,cm^{-2}}$ for CEP of $\varphi_{\mathrm{CEP}} = 0$ and $\varphi_{\mathrm{CEP}} = \pi/2$, measured by VMI. (c) The up (black) and down (red) emission spectra are shown on the left (integration over 40° along the laser polarization) and the asymmetry map $A(W, \varphi_{\mathrm{CEP}})$ that is obtained from such spectra for different CEP values on the right. (d) Phase shift $\varphi_{\mathrm{asymmetry}}$ in the asymmetry $A(W, \theta, \varphi_{\mathrm{CEP}})$ oscillation with φ_{CEP} (only displayed for asymmetry amplitudes larger than 0.07, θ is given with respect to the polarization axis).

The right panel displays the asymmetry map $A(W, \varphi_{\mathrm{CEP}})$. Oscillations of the asymmetry with the CEP are clearly visible above 25 eV that shift in their phase with energy. In the lower energy range, the dependence of the asymmetry on the CEP is more complex and rather weak. These features in the krypton asymmetry data are comparable to what has been observed in argon, which also becomes evident in figure 8(d), where the phase shift $\varphi_{\mathrm{asymmetry}}(W, \theta)$ of the angle-dependent asymmetry oscillation $A(W, \theta, \varphi_{\mathrm{CEP}})$ is shown (for a definition see above). The phase shift is only plotted for significantly high amplitudes of the asymmetry ($A(W, \theta) > 0.07$) and shows a similar angle and energy dependence as was observed for argon (compare figure 3(b)).

Data for xenon for the same pulse parameters are displayed in figure 9. Figures 9(a) and (b) contain inverted images for $\varphi_{\mathrm{CEP}} = 0$ and $\pi/2$, respectively. Note that the angular distributions show strong side-lobes in the plateau range at angles between 30° and 60°. The spectra in the up/down emission direction for $\varphi_{\mathrm{CEP}} = 0$ are shown in figure 9(c) together with the asymmetry map for a phase range of 8π. The plateau region is more pronounced in xenon as has been

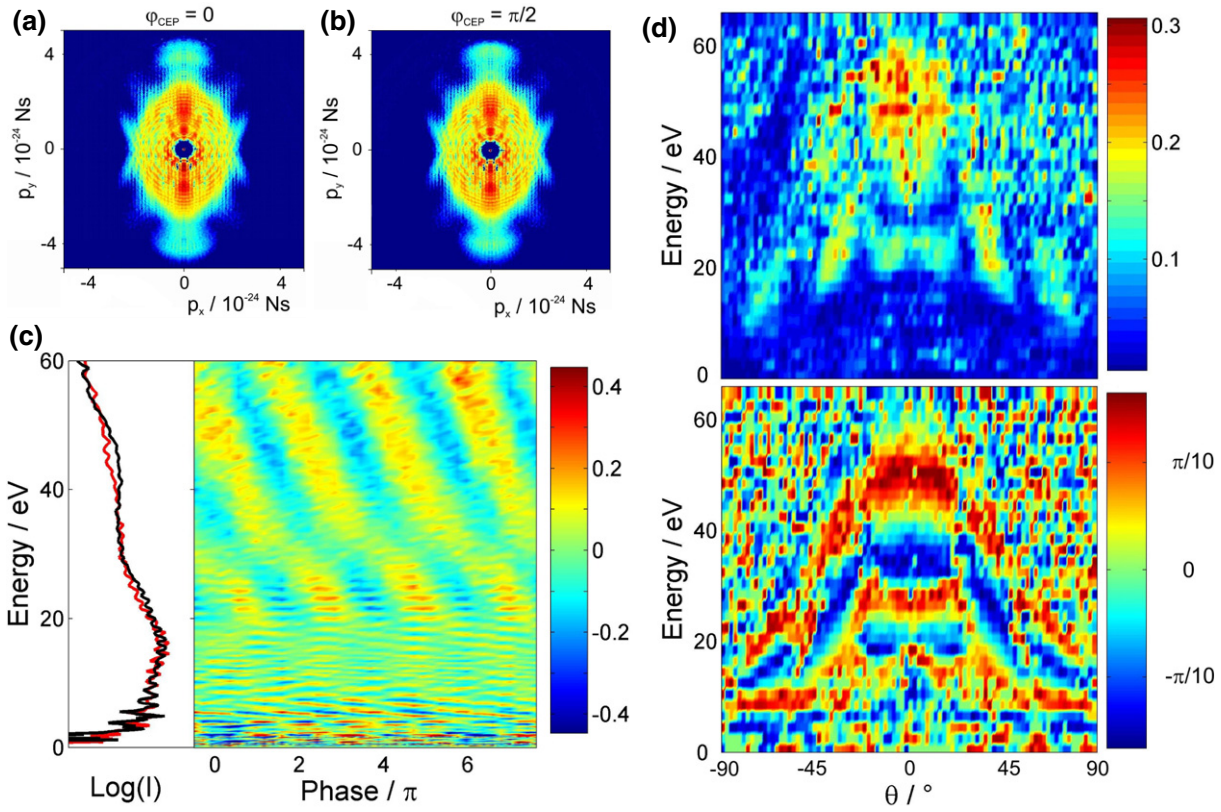

Figure 9. (a), (b) Inverted images for VMI of ATI of xenon with 6 fs laser pulses at $10^{14}\,\mathrm{W\,cm^{-2}}$ for phases of $\varphi_{\mathrm{CEP}} = 0$ and $\varphi_{\mathrm{CEP}} = \pi/2$. (c) The up (black) and down (red) emission spectra are shown on the left (integration over 40° along the laser polarization) and the asymmetry map $A(W, \varphi_{\mathrm{CEP}})$ that is obtained from such spectra for different phase values φ on the right. (d) Amplitude $A_0(W, \theta)$ (upper panel) and phase shift $\varphi_{\mathrm{asymmetry}}$ (lower panel) in the asymmetry $A(W, \theta, \varphi_{\mathrm{CEP}})$ oscillation with φ_{CEP} (θ is given with respect to the polarization axis). As compared to argon and krypton, significant asymmetry is also observed at high emission angles and energies below $2U_{\mathrm{p}}$.

observed earlier [36]. Figure 9(d) shows the amplitude $A_0(W, \theta)$ (upper panel) and phase shift $\varphi_{\mathrm{asymmetry}}(W, \theta)$ (lower panel) of the angle-dependent asymmetry oscillation $A(W, \theta, \varphi_{\mathrm{CEP}})$ for xenon. Clearly, in xenon the asymmetry reaches the highest amplitudes and the CEP dependence is visible all the way down to approximately 5 eV. Two phase jumps are visible in the asymmetry oscillation at about 20 and 30 eV. Above this energy, the patterns are similar to what has been seen already in argon and krypton. At energies below $2U_{\mathrm{p}}$, a significant asymmetry is seen for high emission angles (around 60°). Interestingly, the asymmetry appears strong at angles where side-lobes are observed in the electron emission that were attributed to rescattering contributions. The side-lobes at angles between 30° and 60° from the polarization axis are very pronounced in ATI of xenon. Electrons that undergo rescattering would be expected to depend more strongly on the waveform of the laser field and thus the CEP than directly emitted electrons, which is in accordance with the observation of a significant asymmetry.

6. Towards single-shot mapping of the CEP

The visibility of CEP effects in the range below $2U_p$ for xenon raises the question whether the VMI technique can be used in the limit of a single-shot detection of the phase. Typically in the VMI up to approximately 10^7 electrons cm^{-3} can be created in one laser shot without running into serious space charge problems (i.e. without seeing effects due to the Coulomb repulsion between the created charges, see e.g. [37]). In order to use the VMI as a single-shot phase measurement device, a maximum of up to about 100–100 000 electrons shot^{-1} (depending on the size of the focal volume) needs to be sufficient for determining the CEP from their positions in momentum space. We have performed numerical simulations that are based on the TDSE calculations for argon. We used a Monte Carlo (MC) approach to calculate 'single-shot' cuts through the 3D-momentum images at $p_z = 0$ for a fixed count-rate of N_{count} electrons (note that the MC algorithm creates single-shot images that are weighted by the TDSE-calculated probability that an electron is observed at a particular position in momentum space). Figures 10(a)–(c) show three images that were simulated this way. The MC-algorithm makes use of the symmetry of the images around the polarization p_y-axis and produces half an image for N_{count} electrons, which was mirrored to yield the sample images shown in figure 10. While images with low count numbers only reproduce the strongest features in the 2D-momentum cuts, with a sufficiently high count number the original TDSE calculated images are reproduced.

The CEP φ_{CEP} is determined from such single-shot images by comparison to a set of 40 reference images for CEP from 0 to 2π (such as the ones displayed in figure 5). The comparison between a single-shot image $S(p_x, p_y)$ and a reference image $R(p_x, p_y)$ is done by means of a correlation coefficient C that is defined as follows:

$$C = \sum_x \sum_y \left(\frac{S(p_x, p_y)}{R(p_x, p_y)} - \frac{\overline{S}}{R} \right)^2 . \tag{2}$$

where S/R is the average value of the single-shot images, standardized to the reference image. C will reach a minimum for the best agreement between S and R. Figure 10(a) shows the values of the coefficient C for seven single-shot images with $N_{\text{count}} = 1\,000\,000$ for the set of 40 reference images. For this high number of counts the original CEP (solid line in figure 10(d)) is retrieved very accurately from shot to shot (determined by the minimum value of C). For fewer counts, the noise in the determination of the CEP increases as shown in figure 10(e). The mean value of the CEP that is determined within 100 single-shots and the error (given by 2σ) are given as a function of N_{count}. As an example, the inset shows the determination of the phase by the correlation coefficient for 100 single-shot images at $N_{\text{count}} = 10\,000$. For $N_{\text{count}} \leqslant 10\,000$, outliers are observed that not only determine the noise of the single-shot phase but, as evident for $N_{\text{count}} = 10$–1000, make a determination of the absolute phase (solid line in the figure) impossible. At low numbers $N_{\text{count}} (\leqslant 1000)$, the phase space between 0 and 2π is randomly sampled yielding a mean CEP value close to π. As seen in figure 10(e) for $N_{\text{count}} = 10\,000$ and higher, the simulations indicate that single-shot phase detection with VMI might be possible if a sufficiently high number of electrons can be created without significant space charge effects. Specifically, for $N_{\text{count}} = 100\,000$, we observe that the CEP is retrieved with a standard deviation σ of 210 mrad, which would be satisfactory for most practical purposes.

It is interesting to compare the discussed phase retrieval by VMI of ATI with other methods. Very good accuracy in phase retrieval was claimed by Haworth *et al* [13] using half-cycle cutoffs in high-harmonic generation spectra. They obtained an error of only 50 mrad [13]. An

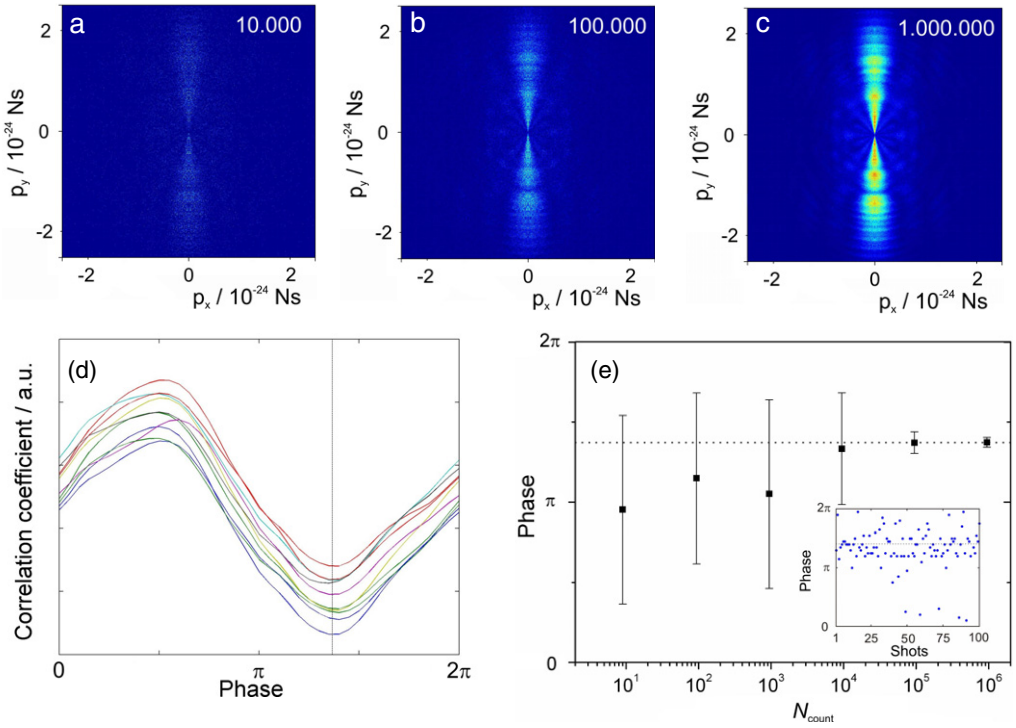

Figure 10. (a)–(c) Single-shot images generated by MC sampling for a given number N_{count}. (d) Correlation coefficient as defined in the text for a set of seven simulated single-shot images and their comparison to a set of 40 reference images for phases between 0 and 2π. The original CEP is indicated by the solid line. (e) Mean value and error in the single-shot CEP determination as a function of N_{count} for a set of 100 single-shot images. The inset shows an example of the single-shot sampling of the phase for $N_{\mathrm{count}} = 10\,000$. The dotted line indicates the original CEP.

error of $3\sigma = 100$ mrad was reported for measurements based on the stereo-ATI method [38]. The information that is used in the stereo-ATI determination of the phase can be viewed as consisting of a subset available with VMI. Therefore, we can expect VMI to reach at least the same accuracy in the determination of the CEP. In addition, CEP effects have clearly been seen in the angular distributions of ATI electrons, such that the availability of this additional information suggests that VMI can be more accurate than stereo-ATI. The error that we obtained at the present stage of our simulations above is certainly limited by (i) the choice of the atomic species and (ii) the comparison of the pictures for various CEP by means of a simple correlation coefficient. Our simulations are based on the TDSE calculations for argon but xenon was found to exhibit stronger CEP effects in the experiments making it desirable to use xenon as a target for VMI phase measurements such as typically done in stereo-ATI determinations of the CEP. We plan to perform TDSE calculations using an accurate Xe potential in the near future. The comparison between a sampled image and a set of reference images for various phases is based here on a simple correlation coefficient. The observed pattern in the shift of the asymmetry oscillations with the electron energy and emission angle (see figures 3(b), 8(d) and 9(d)) indicates that pattern recognition might improve the determination of the CEP from

VMIs. It can also be expected that the currently limited speed at which 2D images can be recorded and processed will be pushed beyond the kilohertz limit in the near future, such that very precise single-shot CEP determination using VMI becomes feasible.

7. Concluding remarks

We have demonstrated that VMI is not only a powerful tool for measuring the full-momentum distributions of ATI in rare gases but also yields and provides a new way to determine the CEP of few-cycle laser pulses from the angular distribution of the emitted electrons. The asymmetry in the emission towards the two sides along the laser polarization direction clearly not only shows a shift in its oscillation with CEP that depends on the kinetic energy of the electrons but also on their emission angle. In the case of xenon, significant asymmetry was observed even below $2U_p$ in particular for high emission angles around 60°. This unique dependence indicates that VMI can also be used instead of stereo-ATI detection to determine the CEP with high accuracy. We have explored the possibility of performing single-shot phase measurements using VMI. MC simulations indicate that CEP retrieval for a sufficiently high number of detected electrons in a single laser shot ($\geqslant$100 000 based on the simulations and analysis procedure presented here) can reveal the single shot CEP with $\sigma < 210$ mrad. So far we have used 'ideal' conditions for these simulations as they were based on 2D-cuts through the momentum distribution and not the measured projections, and furthermore intensity fluctuations of the laser are neglected. The measured data for the three gases argon, krypton and xenon, however, indicate that xenon might be a better candidate for a single-shot VMI detection device as it shows pronounced asymmetries also below $2U_p$, where the number of emitted electrons is orders of magnitudes higher. In addition, we consider our estimation on the maximum number of electrons that can be detected single-shot to be rather conservative, such that also under real experimental conditions, single-shot VMI detection of the CEP seems feasible.

Acknowledgments

We are deeply grateful to Professor Ferenc Krausz for giving us the opportunity to perform the experiments with one of the laser set-ups in his group at MPQ. We further acknowledge the experimental support by Yongfeng Ni, Jafar I Khan, Martin Schultze and Matthias Uiberacker and stimulating discussions of this work with Professors Gerhard Paulus, Wilhelm Becker and Markus Drescher. We thank the European Union for support by the Marie Curie Research Training Network XTRA, MRTN-CT-2003-505138, a Marie Curie Intra-European Fellowship, MEIF-CT-2003-500947, and a European Reintegration Grant (M F K). The research of M F K and M J J V is part of the research program of the 'Stichting voor Fundamenteel Onderzoek der Materie (FOM)', which is financially supported by the 'Nederlandse Organisatie voor Wetenschappelijk Onderzoek (NWO)'. E H and D B M gratefully acknowledge the support by the Volkswagen-Stiftung, by the Ministry of Education and Science, Canton Sarajevo, and by the Federal Ministry of Education and Science, Bosnia and Herzegovina. M F K acknowledges support by the Max-Planck Society and the Emmy-Noether program of the German Science Foundation (DFG).

References

[1] Baltuška A *et al* 2003 *Nature* **421** 611
[2] Kienberger R *et al* 2004 *Nature* **427** 817
[3] Macklin J J *et al* 1993 *Phys. Rev. Lett.* **70** 766
L'Huillier A and Balcou P 1993 *Phys. Rev. Lett.* **70** 774
[4] Lindner F *et al* 2005 *Phys. Rev. Lett.* **95** 040401
[5] Milošević D B *et al* 2003 *Opt. Express* **11** 1418
[6] Paulus G G *et al* 2003 *Phys. Rev. Lett.* **91** 253004
[7] Kling M *et al* 2006 *Science* **312** 246
[8] Goulielmakis E *et al* 2004 *Science* **305** 1267
[9] Apolonski A *et al* 2004 *Phys. Rev. Lett.* **92** 073902
[10] Paulus G G *et al* 2001 *Nature* **414** 182
[11] Verhoef A J *et al* 2006 *Opt. Lett.* **31** 3520
[12] Kreß M *et al* 2006 *Nat. Phys.* **2** 327
[13] Haworth C A *et al* 2007 *Nat. Phys.* **3** 52
[14] Becker W *et al* 2002 *Adv. At. Mol. Opt. Phys.* **48** 35
[15] Milošević D B *et al* 2006 *J. Phys. B: At. Mol. Opt. Phys.* **39** R203
[16] Gallagher T F 1988 *Phys. Rev. Lett.* **61** 2304
Corkum P B *et al* 1989 *Phys. Rev. Lett.* **62** 1259
[17] Walker B *et al* 1994 *Phys. Rev. Lett.* **73** 1227
Schafer K J *et al* 1993 *Phys. Rev. Lett.* **70** 1599
[18] Yang B *et al* 1993 *Phys. Rev. Lett.* **71** 3770
[19] Paulus G G *et al* 1994 *J. Phys. B: At. Mol. Opt. Phys.* **27** L703
[20] Milošević D B *et al* 2002 *Phys. Rev. Lett.* **89** 153001
[21] Remetter T *et al* 2006 *Nat. Phys.* **2** 323
Varjú K *et al* 2006 *J. Phys. B: At. Mol. Opt. Phys.* **39** 3983
[22] Spanner M *et al* 2004 *J. Phys. B: At. Mol. Opt. Phys.* **37** L243
[23] Chandler D W and Houston P L 1987 *J. Chem. Phys.* **87** 1445
[24] Eppink A T J B and Parker D H 1997 *Rev. Sci. Instrum.* **68** 3477
[25] Vrakking M J J 2001 *Rev. Sci. Instrum.* **72** 4084
[26] Schyja V *et al* 1998 *Phys. Rev.* A **57** 3692
[27] Nandor M *et al* 1998 *J. Phys. B: At. Mol. Opt. Phys.* **31** 4617
[28] Paulus G G *et al* 1994 *Europhys. Lett.* **27** 267
[29] Becker W *et al* 1994 *J. Phys. B: At. Mol. Opt. Phys.* **27** L325
Becker W *et al* 1995 *J. Phys. B: At. Mol. Opt. Phys.* **28** 1931
[30] Rauschenberger J *et al* 2006 *Laser Phys. Lett.* **3** 37
Paulus G G *et al* 2004 *Phys. Scr.* T **110** 120
[31] Keldysh L V 1965 *Sov. Phys.—JETP* **20** 1307
Faisal F H M 1973 *J. Phys. B: At. Mol. Phys.* **6** L89
Reiss H R 1980 *Phys. Rev.* A **22** 1786
[32] Milošević D B and Ehlotzky F 2003 *Adv. At. Mol. Opt. Phys.* **49** 373
[33] Hasović E *et al* 2007 *Laser Phys.* **17** 376
[34] Milošević D B *et al* 2003 *Phys. Rev.* A **68** 050702
Gazibegović-Busuladžić A *et al* 2004 *Phys. Rev.* A **70** 053403
[35] Bauer D *et al* 2006 *J. Mod. Opt.* **53** 135
Milošević D B *et al* 2004 *Laser Phys. Lett.* **1** 93
[36] Grasbon F *et al* 2003 *Phys. Rev. Lett.* **91** 173003
[37] Bordas C and Pinare J C 1998 *Phys. Rev.* A **57** R681
[38] Paulus G G 2005 *Laser Phys.* **15** 843